J. Appl. Comput. Mech., xx(x) (2026) 1-15
DOI: 10.22055/jacm.2026.49215.5812

ISSN: 2383-4536
jacm.scu.ac.ir

Shahid Chamran University of Ahvaz

Journal of Applied and Computational Mechanics

Research Paper

Numerical Analysis of Asynchronous Time Scheme for Explicit-Implicit Problems

Radim Dvořák[1,2], Radek Kolman[1]

[1] Institute of Thermomechanics of the CAS, v. v. i., Dolejškova 1402/5, 182 00 Praha 8, Czech Republic, Email: radimd@it.cas.cz (R.D.); kolman@it.cas.cz (R.K.)

[2] CTU in Prague Faculty of Transportation Sciences, Department of Mechanics and Materials, Na Florenci 25, 110 00 Praha 1, Czech Republic, Email: dvorara9@fd.cvut.cz

Received March 25 2026; Revised May 15 2026; Accepted for publication May 18 2026.
✉ Corresponding author: R. Dvořák (dvorara9@fd.cvut.cz)

Abstract. We present an asynchronous time integration framework for partitioned elastodynamic problems, where each subdomain advances with its own local time step. The strong formulation of partitioned elastodynamics is introduced, followed by a weak formulation that couples subdomains via localized Lagrange multipliers acting on accelerations and using linear shape functions, effectively resulting in a generalized mortar approach. After recapitulating the standard direct solution of the equations of motion and our asynchronous scheme for explicit integration, we investigate the dynamics of a small body attached to a larger structure. Three variants of subdomain integration are examined: explicit-explicit, implicit-implicit, and mixed explicit-implicit coupling. Their influence on solution accuracy, energy conservation, and drifting between subdomains is analyzed, with the results validated through comparisons with LS-DYNA simulations. The study highlights that accuracy is well preserved in the explicit-explicit case, while the other variants exhibit measurable drifting that is carefully quantified. Overall, we demonstrate that the proposed asynchronous integration scheme can provide substantial computational speedups in heterogeneous domains, highlighting its potential for efficient simulation of systems with localized fast dynamics.

Keywords: Direct time integration; Finite element method; Asynchronous scheme; Explicit-implicit; Wave propagation.

1. Introduction

Elastodynamic problems arise in a wide range of scientific and engineering applications, including seismic wave propagation, structural dynamics, impact analysis, and nondestructive testing. These problems are characterized by the propagation of stress waves governed by hyperbolic partial differential equations, often requiring high spatial and temporal resolution to accurately capture transient phenomena. As a result, large-scale elastodynamic simulations pose significant computational challenges, particularly when high-frequency content, heterogeneous materials, or complex geometries are involved.

In the case of linear structural behavior, reduced-order approaches based on modal superposition are frequently employed due to their high computational efficiency, particularly in real-time simulations and repeated analyses [1]. However, direct time integration methods have remained the predominant approach for solving elastodynamic equations [2], especially in applications involving complex geometries, localized nonlinearities, or transient wave propagation phenomena. Explicit and implicit schemes, such as Newmark-type methods or generalized-α formulations, provide robust and well-understood frameworks for advancing the solution in time.

Numerous time integration schemes have been developed for structural dynamics, focusing on improving numerical dissipation, stability, and energy conservation properties [3, 4]. However, these methods are typically formulated for a single global time step and are not directly applicable to problems involving multiple time scales across partitioned domains.

However, the inherently sequential nature of classical time-stepping limits scalability, as each time step depends on the solution from the previous one. While spatial parallelization has been extensively exploited through domain decomposition techniques, the time dimension has traditionally remained a bottleneck in large-scale simulations.

To overcome this limitation, parallel-in-time integration methods have been developed as a complementary strategy to spatial parallelism. Techniques such as Parareal [5], multigrid-in-time [6], and related algorithms aim to distribute the computational workload across the temporal domain, enabling concurrency beyond what is achievable through spatial decomposition alone. When combined with domain decomposition in space, these methods offer the potential for substantial reductions in wall-clock time for large elastodynamic simulations. However, the effectiveness of combined space-time parallelization is strongly influenced by the heterogeneity of the computational domain. In domain-decomposed elastodynamic problems, subdomains may differ significantly in material properties, mesh resolution, stability constraints, or local wave speeds. Consequently, the most complex or restrictive subdomain (typically characterized by the smallest admissible time step or the highest computational cost per step) dictates the overall pace of the simulation.

Published online: July 06 2026

In this context, asynchronous schemes represent an effective approach for direct time integration. Early contributions by Belytschko and Mullen [7, 8] and Smolinski et al. [9], dating back to the second half of the 20th century, introduced the concept of non-uniform time stepping. These works were followed by several important studies addressing stability and accuracy aspects [10, 11]. However, these early approaches were formulated without domain decomposition and thus lacked a consistent framework for coupling subdomains with different time scales.

More recent developments incorporate domain decomposition techniques combined with Lagrange multipliers to enforce kinematic interface constraints. A widely used approach was proposed by Combescure and Gravouil [12] and later implemented in Europlexus [13]. This method allowed arbitrary and time-varying time steps across subdomains, but introduces artificial interface dissipation. Energy-conserving extensions were subsequently developed by Prakash and Hjelmstad [14] and Fekak et al. [15], although these are generally restricted to integer ratios of time steps.

Multi-time-step strategies combining explicit and implicit schemes have also been proposed to address localized non-smooth phenomena [16], particularly in impact simulations. Such approaches enable different time integration schemes and time steps in different subdomains, leading to significant computational savings. Nevertheless, they are typically tailored to specific applications or coupling strategies, and a general framework for asynchronous partitioned elastodynamics remains an open challenge.

Further developments include the BGC macro-micro approach introduced by Gravouil et al. [17], which employed linear interpolation of Lagrange multipliers. The macro formulation is energy-conserving but requires a global solution, whereas the micro formulation is explicit but introduces dissipation. Related global formulations have been proposed by Subber and Matouš [18] and by Seibold and Rixen [19], both of which relied on common time levels and involve large global solves. In general, methods based on velocity continuity and linear interpolation [17] may suffer from interface drifting. An alternative approach enforcing acceleration continuity was proposed by Cho et al. [20], although it was likewise limited to integer time-step ratios.

Asynchronous time integration has also been explored to alleviate severe time-step restrictions imposed by fine spatial discretizations. For instance, asynchronous variational integrators allowed individual elements to evolve with independent time steps, significantly improving efficiency in dynamic fracture simulations [21]. However, such formulations are typically defined at the element level and are not directly applicable to partitioned multi-domain problems involving heterogeneous solvers and coupling conditions.

More generally, asynchronous time-stepping strategies have been developed in other fields to handle stiff systems with multiple time scales [22], demonstrating substantial computational gains over classical time integration methods. Nevertheless, their extension to partitioned elastodynamic systems with consistent subdomain coupling remains non-trivial.

It can be observed that all of the aforementioned methods suffer from certain restrictions or limitations. In our previous work [23], we developed an asynchronous time integration framework that overcomes these issues. In the proposed algorithm, each subdomain is advanced using its own local time step while employing the same explicit integration scheme across all subdomains. That study focused on the formulation and stability of the asynchronous integration and did not address heterogeneous integration schemes or potential computational speedups.

In the present paper, we extend this methodology in several ways. First, we introduce explicit-implicit coupling, allowing different subdomains to use integration schemes tailored to their local dynamics. Second, we address the issue of drifting between subdomains and analyze its impact on solution accuracy. Finally, we demonstrate how asynchronous integration can produce significant computational speedups in problems with highly heterogeneous subdomains, such as localized impacts or small, fast-moving regions interacting with larger, slower domains.

The paper begins with the strong formulation of partitioned elastodynamics (Section 2), introducing the governing equations and the interface conditions that connect interacting subdomains. This is followed by the finite element discretization using extended localized Lagrange multipliers (Section 3), which establishes a generalized mortar framework to couple subdomains via accelerations. The direct solution of the equations of motion is then revisited in Section 4, focusing on the frame problem and on the individual i-th subdomain problem, thereby forming the foundation for the asynchronous approach. Section 5 discusses temporal discretization via direct time integration methods, reviewing explicit and implicit schemes within this partitioned framework, while Section 6 presents the concept of interface separation by system reduction, enabling efficient solution of the frame and surrounding interface regions independently of the full system. In Section 7, the problem of drifting between subdomains is discussed, paving the way for Section 8, which details the asynchronous integration algorithm for two subdomains connected via a single frame. Section 9 presents a computational analysis of a small body attached to a larger structure, comparing explicit-explicit, implicit-implicit, and mixed explicit-implicit variants, while monitoring energy, drift, and computational speedup, also with respect to LS-DYNA. The paper concludes in Section 10.

2. Strong Formulation of Partitioned Elasto-Dynamics

In this section, the variational formulation of partitioned elastodynamics is introduced. For illustrative purposes, we consider a scenario involving two elastic subdomains (see Fig. 1), where $\boldsymbol{\sigma}_i(\boldsymbol{x})$ denotes the stress tensor, $\boldsymbol{t}_i(\boldsymbol{x})$ denotes the traction vector, $\boldsymbol{u}_i(\boldsymbol{x})$ describes the displacement field, and $\boldsymbol{x} \in \boldsymbol{\Omega}$ indicates the position of a material point. The symbol $\boldsymbol{\Omega}$ denotes the spatial domain, which is divided into two subdomains $\boldsymbol{\Omega_i}, \boldsymbol{i} = \mathbf{1}, \mathbf{2}$.

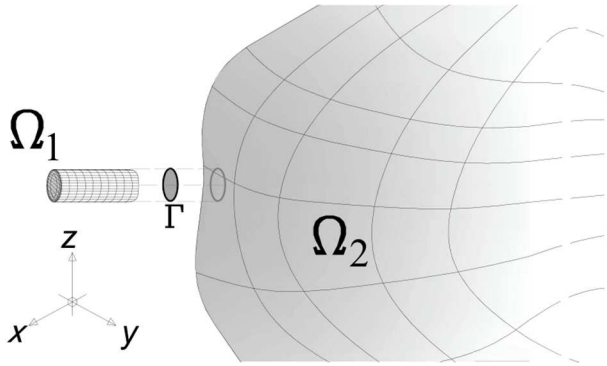

Fig. 1. Illustration of a domain Ω partitioned into two subdomains Ω_i with a shared interface Γ.

For these non-overlapping subdomains, we have:

$$\boldsymbol{\Omega}_1 \cup \boldsymbol{\Omega}_2 = \boldsymbol{\Omega} \ , \qquad \boldsymbol{\Omega}_1 \cap \boldsymbol{\Omega}_2 = \emptyset \tag{1}$$

sharing a common interface $\boldsymbol{\Gamma}$, with normal $\mathbf{n}_{\boldsymbol{\Gamma}}$, where the compatibility constraint is expressed:

$$\ddot{\boldsymbol{u}}_i(\boldsymbol{x}) = \ddot{\boldsymbol{u}}_{\boldsymbol{\Gamma}}(\boldsymbol{x}) \ , \qquad \boldsymbol{x} \in \Gamma \ , \tag{2}$$

where $\ddot{\boldsymbol{u}}_{\boldsymbol{\Gamma}}(\boldsymbol{x})$ is the interface acceleration field.

2.1. Partitioned equations for a linear structural system - weak one-for-all formulation

Based on Hamilton's principle for partitioned constrained elasto-dynamics we use the variational formulation proposed by Park and Felippa [24, 25]. The variational form of the Hamiltonian can be written using the following three-field expression [26]:

$$\delta\mathcal{H}(\boldsymbol{u}, \boldsymbol{u}_\Gamma, \boldsymbol{\ell}) = \int_0^T \delta \left\{ \sum_{i=1}^{2} \{\mathcal{T}_i(\boldsymbol{u}) - \ \mathcal{U}_i(\boldsymbol{u}) + \ \mathcal{W}_i(\boldsymbol{u})\} \ + \ \mathcal{W}_\Gamma(\boldsymbol{u}, \boldsymbol{u}_\Gamma, \boldsymbol{\ell}) \right\} dt = 0 \ , \tag{3}$$

where,

$$\delta\mathcal{T}_i = \int_{\Omega_i} \delta\dot{\boldsymbol{u}}_i \cdot \rho\dot{\boldsymbol{u}}_i \, dV \ , \qquad \delta\mathcal{U}_i = \int_{\Omega_i} \delta\boldsymbol{\varepsilon}_i : \boldsymbol{\sigma}_i \, dV \ , \qquad \delta\mathcal{W}_i = \int_{\Omega_i} \delta\boldsymbol{u}_i \cdot \boldsymbol{b}_i \, dV \ + \ \int_{\partial\Omega_i^N} \delta\boldsymbol{u}_i \cdot \boldsymbol{t}_i \, dS \tag{4}$$

stands for the virtual kinetic and potential energy and for the virtual work done by external loads, where $\boldsymbol{\sigma}$ is the stress tensor, $\boldsymbol{\varepsilon}$ is the infinitesimal strain tensor, ρ is the mass density, $\boldsymbol{b}$ is the vector of the intensity of the volume forces, $\boldsymbol{u}$ is the displacement field and $\boldsymbol{t}$ is given traction. The last term of Eq. (3) represents the virtual work of the interface constraints:

$$\delta\mathcal{W}_\Gamma(\boldsymbol{u}, \boldsymbol{u}_\Gamma, \boldsymbol{\ell}) = \sum_{1=1}^{2} \int_\Gamma \delta[\boldsymbol{\ell}_i(\boldsymbol{u}_i - \boldsymbol{u}_\Gamma)] \, dS \ , \tag{5}$$

where the vector fields $\boldsymbol{u}_i(\boldsymbol{x}, t)$ and $\boldsymbol{\ell}_i(\boldsymbol{x}, t)$ represent the displacement and localized Lagrange multipliers of the i-th subdomain, respectively, $\boldsymbol{u}_{\boldsymbol{\Gamma}}(\boldsymbol{x}, t)$ represents the frame displacement (see Fig. 2).

3. Discretization via FEM Using Extended LLM

In problems involving non-matching meshes across adjacent subdomains, the accurate transfer of kinematic and dynamic quantities across interfaces represents an important challenge. Besides classical finite element formulations, isogeometric analysis has also been identified as a promising approach for improving geometric continuity and interface representation in complex multiphysics and coupled problems [27]. In the present work, however, a standard finite element discretization is adopted. The spatial discretization by the finite element method is defined for each subdomain $\boldsymbol{\Omega_i}$ and frame $\boldsymbol{\Gamma}$ as:

$$\begin{aligned} \boldsymbol{u}_i(\boldsymbol{x}) &= \mathbf{N}_{u_i}(\boldsymbol{x}) \ \mathbf{u}_i \ , \\ \boldsymbol{\ell}_i(\boldsymbol{x}) &= \mathbf{N}_{\lambda_i}(\boldsymbol{x}) \ \boldsymbol{\lambda}_i \ , \\ \mathbf{u}_\Gamma(\boldsymbol{x}) &= \mathbf{N}_{u_\Gamma}(\boldsymbol{x}) \ \mathbf{u}_\Gamma \ , \end{aligned} \tag{6}$$

where $\mathbf{N}_{u_i}$, $\mathbf{N}_{\lambda_i}$ and $\mathbf{N}_{u_\Gamma}$ are appropriate shape functions and $\mathbf{u}_i$, $\boldsymbol{\lambda}_i$, $\mathbf{u}_\Gamma$ are nodal unknowns. Depending on the form of shape functions, we distinguish different methods of domain decomposition [28]. In the present work, we employ the method of Localized Lagrange Multipliers (LLM). However, instead of its classical form [29, 30], which uses Dirac delta shape functions for the multipliers, we adopt the shape functions of the nodal displacements:

$$\boldsymbol{\ell}_i(\boldsymbol{x}) = [\mathbf{N}_{u_i}\mathbf{B}_i](\boldsymbol{x}) \ \boldsymbol{\lambda}_i \ , \tag{7}$$

where $\mathbf{B}_i$ is Boolean operator picking only those degrees of freedom interacting with the frame $\boldsymbol{\Gamma}$. Moreover, we adopt subdomain's 1 mesh also for the frame discretization:

$$\boldsymbol{u}_\Gamma(\boldsymbol{x}) = [\mathbf{N}_{u_1}\mathbf{B}_1](\boldsymbol{x}) \ \mathbf{u}_\Gamma \ , \tag{8}$$

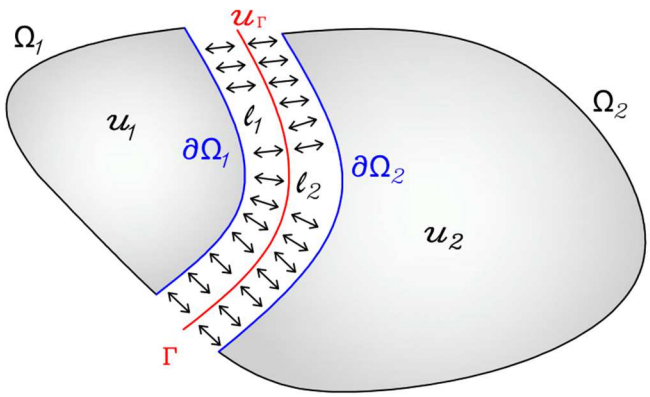

Fig. 2. Domain of dependence/influence of the frame.

This helps us avoid the otherwise complex process of selecting frame node coordinates using some of the existing methods [31-34], which are applicable only in particular cases and generally do not guarantee satisfaction of the patch test.

Introducing the discretization into the variational form (3), the problem is transformed to a second-order semi-discrete system:

$$\begin{bmatrix} \overline{\mathbf{K}} & \mathbf{B}\,\mathbf{M}^{\mathrm{B}} & \mathbf{0} \\ \mathbf{M}^{\mathrm{B}^{\mathrm{T}}}\mathbf{B}^{\mathrm{T}} & \mathbf{0} & -\mathbf{C}_{\lambda u_\Gamma} \\ \mathbf{0} & -\mathbf{C}_{\lambda u_\Gamma}^{\mathrm{T}} & \mathbf{0} \end{bmatrix} \begin{Bmatrix} \mathbf{u} \\ \boldsymbol{\lambda} \\ \mathbf{u}_\Gamma \end{Bmatrix} = \begin{Bmatrix} \mathbf{f} \\ \mathbf{0} \\ \mathbf{0} \end{Bmatrix}, \tag{9}$$

where,

$$\overline{\mathbf{K}} = \mathbf{M}\,\mathrm{D}^2 + \mathbf{K}\,, \qquad \mathrm{D} = \frac{d}{dt}\,,$$

where we recognize equation of motion, kinematic interface constraints and interface equilibrium condition. The matrices $\mathbf{M}$ and $\mathbf{K}$ in Eq. (9) are the global mass matrix and the global stiffness matrix, respectively, and $\mathbf{f}$ is the block vector of external load:

$$\mathbf{M} = \begin{bmatrix} \mathbf{M}_1 & \\ & \mathbf{M}_2 \end{bmatrix}, \qquad \mathbf{K} = \begin{bmatrix} \mathbf{K}_1 & \\ & \mathbf{K}_2 \end{bmatrix}, \qquad \mathbf{f} = \begin{bmatrix} \mathbf{f}_1 \\ \mathbf{f}_2 \end{bmatrix}, \tag{10}$$

where the i-th subdomain structural matrices and load vector, with given discretization of Eq. (6), are expressed as:

$$\begin{aligned} \mathbf{M}_i &= \int_{\Omega_i} \rho \mathbf{N}_{u_i}^{\mathrm{T}}\, \mathbf{N}_{u_i}\, dV\,, \\ \mathbf{K}_i &= \int_{\Omega_i} \mathbf{N}'_{u_i}{}^{\mathrm{T}}\, \mathbf{D}_i\, \mathbf{N}'_{u_i}\, dV\,, \\ \mathbf{f}_i &= \int_{\Omega_i} \mathbf{N}_{u_i}^{\mathrm{T}}\, \boldsymbol{b}_i\; dV \;+\; \int_{\partial\Omega_i^N} \mathbf{N}_{u_i}^{\mathrm{T}}\, \boldsymbol{t}_i\; dS\,, \end{aligned} \tag{11}$$

where ρ is mass density, $\mathbf{N}'_{u_i}$ is first derivative of displacement shape functions, and $\mathbf{D}_i$ is subdomain material matrix. The vector $\boldsymbol{\lambda}$ is the block vector of Lagrange multipliers:

$$\boldsymbol{\lambda} = \begin{bmatrix} \boldsymbol{\lambda}_1 \\ \boldsymbol{\lambda}_2 \end{bmatrix} \tag{12}$$

and $\mathbf{u}_\Gamma$ is the vector of frame displacement. Matrix $\mathbf{B}$ is block diagonal matrix:

$$\mathbf{B} = \begin{bmatrix} \mathbf{B}_1 & \\ & \mathbf{B}_2 \end{bmatrix}. \tag{13}$$

Finally, the matrices $\mathbf{M}^{\mathrm{B}}$ and $\mathbf{C}_{\lambda u_\Gamma}$ in Eq. (9) provide subdomain-frame interaction and consist of submatrices:

$$\mathbf{M}^{\mathrm{B}} = \begin{bmatrix} \mathbf{M}_{11}^{\mathrm{B}} & \\ & \mathbf{M}_{22}^{\mathrm{B}} \end{bmatrix}, \qquad \mathbf{C}_{\lambda u_\Gamma} = \begin{bmatrix} \mathbf{M}_{11}^{\mathrm{B}} \\ \mathbf{M}_{12}^{\mathrm{B}} \end{bmatrix}, \tag{14}$$

where,

$$\mathbf{M}_{ii}^{\mathrm{B}} = \int_\Gamma \left\{ \left[\mathbf{N}_{u_i}\ \mathbf{B}_i\right]^{\mathrm{T}}\ \left[\mathbf{N}_{\lambda_i}\right] \right\} dS = \int_\Gamma \left\{ \left[\mathbf{N}_{u_i}\ \mathbf{B}_i\right]^{\mathrm{T}}\ \left[\mathbf{N}_{u_i}\ \mathbf{B}_i\right] \right\} dS \tag{15}$$

is the i-th subdomain boundary interface mass matrix and:

$$\mathbf{M}_{12}^{\mathrm{B}} = \int_\Gamma \{\mathbf{N}_{\lambda_1}^{\mathrm{T}}\ \mathbf{N}_{u_\Gamma}\}\ dS = \int_\Gamma \{[\mathbf{N}_{u_1}\ \mathbf{B}_1]^{\mathrm{T}}\ [\mathbf{N}_{u_2}\ \mathbf{B}_2]\}\ dS \tag{16}$$

is the coupling operator obtained by a well-known subroutine of the Mortar method - a projection of slave and master nodes onto the common interface, calculation of polygon clipping, division of the clip polygon into triangular integration cells, and performing Gaussian integration. Here, we evaluate only one operator $\mathbf{M}_{12}$ thanks to the wise pick of multipliers and frame shape functions.

3.1. Final system form

We now extract the system of governing equations from Eq. (9), which will be used in the subsequent developments. In order to solve the system, we apply the second time derivative to the displacement constraints, whereby the second equation becomes a condition enforcing acceleration continuity, so the final form is:

$$\mathbf{M}\,\ddot{\mathbf{u}} + \mathbf{K}\,\mathbf{u} = \mathbf{f} - \mathbf{B}\,\mathbf{M}^{\mathrm{B}}\,\boldsymbol{\lambda} \quad \text{as the Equation of motion,} \tag{17}$$

$$\mathbf{M}^{\mathrm{B}^{\mathrm{T}}}\mathbf{B}^{\mathrm{T}}\,\ddot{\mathbf{u}} - \mathbf{C}_{\lambda u_\Gamma}\,\ddot{\mathbf{u}}_\Gamma = \mathbf{0} \quad \text{as the Kinematic interface constraints,} \tag{18}$$

$$\mathbf{C}_{\lambda u_\Gamma}^{\mathrm{T}} = \mathbf{0} \quad \text{as the Interface equilibrium condition.} \tag{19}$$

where we have four unknown vectors; nodal acceleration $\ddot{\mathbf{u}}$ and displacement $\mathbf{u}$ interconnected via time disretization, frame acceleration $\ddot{\mathbf{u}}_\Gamma$ and Lagrange multipliers $\boldsymbol{\lambda}$. Note that displacement and velocity continuity are no longer enforced, and drift (see Sec. 7) will occur in both fields. Although the majority of existing methods consider coupling at the velocity level [12, 13], thereby eliminating drift in the velocity field, we prefer to couple the subdomains at the acceleration level. This choice enables straightforward derivation of explicit expressions for the frame and interface variables within the asynchronous framework. In this way, there is no need to introduce temporal linear interpolation of the Lagrange multipliers, and all unknowns can be consistently obtained directly from the equations of motion.

4. Direct Solution of the Equation of Motion

The solution of the problem consists of two parts:

- the frame problem, i.e., obtaining the frame acceleration $\ddot{\mathbf{u}}_\Gamma$ (and therefore the Lagrange multipliers $\boldsymbol{\lambda}$), and
- the domain problem, i.e., obtaining the actual acceleration $\ddot{\mathbf{u}}$ of the domain (subdomains).

4.1. The frame problem

Let us define the acceleration predictor $\tilde{\ddot{\mathbf{u}}}$, which evaluates the acceleration of the subdomains as if they were free-floating bodies without mutual constraints:

$$\tilde{\ddot{\mathbf{u}}} = \mathbf{M}^{-1}(\mathbf{f} - \mathbf{K}\ \mathbf{u})\ . \tag{20}$$

By comparing Eq. (20) with original equation of motion, Eq. (17), we see that:

$$\tilde{\ddot{\mathbf{u}}} = \ddot{\mathbf{u}} + \mathbf{M^{-1}B}\ \mathbf{M}^{\mathrm{B}}\ \boldsymbol{\lambda}\ , \tag{21}$$

i.e., multiplied by $\mathbf{M}^{\mathrm{B}^{\mathrm{T}}}\mathbf{B}^{\mathrm{T}}$ from the left and with reorganized order:

$$\mathbf{M}^{\mathrm{B}^{\mathrm{T}}}\mathbf{B}^{\mathrm{T}}\ddot{\mathbf{u}} = \mathbf{M}^{\mathrm{B}^{\mathrm{T}}}\mathbf{B}^{\mathrm{T}}\ \tilde{\ddot{\mathbf{u}}} - \ \mathbf{M}^{\mathrm{B}^{\mathrm{T}}}\mathbf{B}^{\mathrm{T}}\mathbf{M^{-1}B}\ \mathbf{M}^{\mathrm{B}}\ \boldsymbol{\lambda}\ , \tag{22}$$

which can be directly substituted for the first term of the kinematic interface constraints, Eq. (18), so we obtain:

$$\mathbf{M}^{\mathrm{B}^{\mathrm{T}}}\mathbf{B}^{\mathrm{T}}\ \tilde{\ddot{\mathbf{u}}} - \mathbf{M}^{\mathrm{B}^{\mathrm{T}}}\mathbf{B}^{\mathrm{T}}\mathbf{M^{-1}B}\ \mathbf{M}^{\mathrm{B}}\ \boldsymbol{\lambda} - \mathbf{C}_{\lambda u_\Gamma}\ \ddot{\mathbf{u}}_\Gamma = \mathbf{0}\ \ , \tag{23}$$

which is the equation of motion of the frame. Now, we do the final touch by multiplying this equation by $\mathbf{C}^{\mathrm{T}}_{\lambda u_\Gamma}(\mathbf{M}^{\mathrm{B}^{\mathrm{T}}}\mathbf{B}^{\mathrm{T}}\mathbf{M^{-1}B}\ \mathbf{M}^{\mathrm{B}})^{-1}$ from the left:

$$\mathbf{C}^{\mathrm{T}}_{\lambda u_\Gamma}(\mathbf{M}^{\mathrm{B}^{\mathrm{T}}}\mathbf{B}^{\mathrm{T}}\mathbf{M^{-1}B}\ \mathbf{M}^{\mathrm{B}})^{-1}\mathbf{M}^{\mathrm{B}^{\mathrm{T}}}\mathbf{B}^{\mathrm{T}}\ \tilde{\ddot{\mathbf{u}}}\ - \mathbf{C}^{\mathrm{T}}_{\lambda u_\Gamma}\ \boldsymbol{\lambda} - \ \mathbf{C}^{\mathrm{T}}_{\lambda u_\Gamma}(\mathbf{M}^{\mathrm{B}^{\mathrm{T}}}\mathbf{B}^{\mathrm{T}}\mathbf{M^{-1}B}\ \mathbf{M}^{\mathrm{B}})^{-1}\mathbf{C}_{\lambda u_\Gamma}\ \ddot{\mathbf{u}}_\Gamma = \mathbf{0}\ , \tag{24}$$

so, we can recognize the second term as the condition of interface equilibrium, Eq. (19), which allows us to eliminate the multipliers and finally express the frame acceleration:

$$\ddot{\mathbf{u}}_\Gamma = \left[\mathbf{C}^{\mathrm{T}}_{\lambda u_\Gamma}(\mathbf{M}^{\mathrm{B}^{\mathrm{T}}}\mathbf{B}^{\mathrm{T}}\mathbf{M^{-1}B}\ \mathbf{M}^{\mathrm{B}})^{-1}\mathbf{C}_{\lambda u_\Gamma}\right]^{-1} \cdot \left[\mathbf{C}^{\mathrm{T}}_{\lambda u_\Gamma}(\mathbf{M}^{\mathrm{B}^{\mathrm{T}}}\mathbf{B}^{\mathrm{T}}\mathbf{M^{-1}B}\ \mathbf{M}^{\mathrm{B}})^{-1}\mathbf{M}^{\mathrm{B}^{\mathrm{T}}}\mathbf{B}^{\mathrm{T}}\ \tilde{\ddot{\mathbf{u}}}\right] \tag{25}$$

explicitly. Thanks to the block diagonal form of the inverse coefficient matrix in Eq. (25), we can use the sum notation:

$$\ddot{\mathbf{u}}_\Gamma = \left[\sum_{i=1}^{2}\left\{\mathbf{M}^{\mathrm{B}^{\mathrm{T}}}_{1i}(\mathbf{M}^{\mathrm{B}^{\mathrm{T}}}_{ii}\mathbf{B}^{\mathrm{T}}_i\mathbf{M}^{-\mathbf{1}}_i\mathbf{B}_i\mathbf{M}^{\mathrm{B}}_{ii})^{-1}\mathbf{M}^{\mathrm{B}}_{1i}\right\}\right]^{-1} \bullet \sum_{i=1}^{2}\left\{\mathbf{M}^{\mathrm{B}^{\mathrm{T}}}_{1i}(\mathbf{M}^{\mathrm{B}^{\mathrm{T}}}_{ii}\mathbf{B}^{\mathrm{T}}_i\mathbf{M}^{-\mathbf{1}}_i\mathbf{B}_i\mathbf{M}^{\mathrm{B}}_{ii})^{-1}\ \mathbf{M}^{\mathrm{B}^{\mathrm{T}}}_{ii}\mathbf{B}^{\mathrm{T}}_i\ \tilde{\ddot{\mathbf{u}}}_i\right\} \tag{26}$$

and express the acceleration of the frame:

$$\ddot{\mathbf{u}}_\Gamma = \mathbf{M}^{-1}_\Gamma\ \mathbf{f}_\Gamma\ , \tag{27}$$

where,

$$\begin{aligned}\mathbf{M}^{-1}_\Gamma &= \left[\sum_{i=1}^{2}\left\{\mathbf{M}^{\mathrm{B}^{\mathrm{T}}}_{1i}(\mathbf{M}^{\mathrm{B}^{\mathrm{T}}}_{ii}\mathbf{B}^{\mathrm{T}}_i\mathbf{M}^{-\mathbf{1}}_i\mathbf{B}_i\mathbf{M}^{\mathrm{B}}_{ii})^{-1}\mathbf{M}^{\mathrm{B}}_{1i}\right\}\right]^{-1}\ ,\\ \mathbf{f}_\Gamma &= \sum_{i=1}^{2}\left\{\mathbf{M}^{\mathrm{B}^{\mathrm{T}}}_{1i}(\mathbf{M}^{\mathrm{B}^{\mathrm{T}}}_{ii}\mathbf{B}^{\mathrm{T}}_i\mathbf{M}^{-\mathbf{1}}_i\mathbf{B}_i\mathbf{M}^{\mathrm{B}}_{ii})^{-1}\ \mathbf{M}^{\mathrm{B}^{\mathrm{T}}}_{ii}\mathbf{B}^{\mathrm{T}}_i\ \tilde{\ddot{\mathbf{u}}}_i\right\}\end{aligned} \tag{28}$$

are the frame mass matrix and frame load vector, respectively.

Remark 1. Note that frame acceleration $\ddot{\mathbf{u}}_\Gamma$ in Eq. (25) depends exclusively on domain's accelerator predictor $\tilde{\ddot{\mathbf{u}}}$ in Eq. (20). This means, that frame motion is directly given by actual state of the subdomains, like they were free floating bodies.

4.2. The i-th subdomain problem

The coefficient matrix of Eq. (23) has block diagonal form. Therefore, once we know frame acceleration, we can obtain i-th Lagrange multipliers from Eq. (23) as:

$$\boldsymbol{\lambda}_i = (\mathbf{M}^{\mathrm{B}^{\mathrm{T}}}_{ii}\mathbf{B}^{\mathrm{T}}_i\mathbf{M}^{-\mathbf{1}}_i\mathbf{B}_i\mathbf{M}^{\mathrm{B}}_{ii})^{-1} \cdot (\ \mathbf{M}^{\mathrm{B}^{\mathrm{T}}}_{ii}\mathbf{B}^{\mathrm{T}}_i\ \tilde{\ddot{\mathbf{u}}}_i - \ \mathbf{M}^{\mathrm{B}}_{1i}\ \ddot{\mathbf{u}}_\Gamma)\ . \tag{29}$$

Then, looking back at Eq. (21),

$$\ddot{\mathbf{u}}_i = \ \tilde{\ddot{\mathbf{u}}}_i - \mathbf{M}^{-\mathbf{1}}_i\mathbf{B}_i\ \mathbf{M}^{\mathrm{B}}_{ii}\ \ \boldsymbol{\lambda}_i \tag{30}$$

is our subdomain acceleration.

5. Temporal Discretization by DTI Methods

For simplicity, we introduce only the basic direct time integration (DTI) methods belonging to the Newmark family, including the central difference method. These methods can be expressed in a unified form, where individual schemes are distinguished by appropriate choices of the parameters β and γ [2]. The discretization is generally performed in the following manner:

1. Predict,

$$(\mathbf{u})^{n+1}_p = (\mathbf{u})^n + \Delta t(\dot{\mathbf{u}})^n + \frac{\Delta t^2}{2}(1-2\beta)(\ddot{\mathbf{u}})^n\ , \tag{31}$$

$$(\dot{\mathbf{u}})_p^{n+1} = (\dot{\mathbf{u}})^n + \Delta t\ (1-\gamma)(\ddot{\mathbf{u}})^n\ ,$$

2. solve the fundamental system in order to obtain its acceleration $(\ddot{\mathbf{u}})^{n+1}$ using the effective mass matrix,

$$\widehat{\mathbf{M}} = (\mathbf{M} + \beta\Delta t^2\mathbf{K})\ , \tag{32}$$

3. and correct,

$$\begin{aligned}(\mathbf{u})^{n+1} &= (\mathbf{u})_p^{n+1} + \beta\ \Delta t^2\ (\ddot{\mathbf{u}})^{n+1}\ ,\\ (\dot{\mathbf{u}})^{n+1} &= (\dot{\mathbf{u}})_p^{n+1} + \gamma\ \Delta t\ (\ddot{\mathbf{u}})^{n+1}\ .\end{aligned} \tag{33}$$

The solution of the semidiscrete system of Eqs. (17)-(19) can be then summarized in the following compact Algorithm 1.

6. Isolation of the Frame by System Reduction

We want to be able to solve the frame $\boldsymbol{\Gamma}$ at least in near future independently from surrounding subdomains $\boldsymbol{\Omega_1}, \boldsymbol{\Omega_2}$. In order to do so, we apply the idea of *domain of dependence* and *domain of influence* in the framework of the wave equation. For a time interval $\epsilon_i\ \Delta t_i^c$, we can define *domain of dependence* of the frame in each subdomain (see Fig. 3), where ϵ_i is the safety factor of subdomain $\boldsymbol{\Omega_i}$ given by relation:

$$\epsilon_i \geq 1 + \Delta t_i/\Delta t_i^c, \tag{34}$$

where Δt_i^c is the theoretical critical time step of the CDM method and Δt_i is the actual computational time step, which may be greater for unconditionally stable DTI methods (e.g., implicit average accelerations). We call these subareas *interface regions* with the notation of $\boldsymbol{\Omega}_i^{\mathbf{r}}$ for $i = 1, 2$.

We obtain i-th interface region connected to the frame by a selective reduction of degrees of freedom. For this purpose, we define the boolean operator $\mathbf{R}$ (transformation matrix) such that:

$$\mathbf{R}\ \mathbf{u} = \begin{bmatrix}\mathbf{R}_1 & \\ & \mathbf{R}_2\end{bmatrix} \cdot \begin{bmatrix}\mathbf{u}_1\\ \mathbf{u}_2\end{bmatrix} = \begin{bmatrix}\mathbf{u}_1^{\mathbf{r}}\\ \mathbf{u}_2^{\mathbf{r}}\end{bmatrix} = \mathbf{u}^{\mathbf{r}}\ . \tag{35}$$

By the substitution of the following transformation:

$$\mathbf{u} = \mathbf{R}^{\mathrm{T}}\mathbf{u}^{\mathbf{r}} \tag{36}$$

into the governing system of Eq. (9) and by multiplying the first equation by operator $\mathbf{R}$ we obtain the reduced problem.

Step 1. Predict $\{\mathbf{u}, \dot{\mathbf{u}}\}_p^{n+1}$ from $\{\mathbf{u}, \dot{\mathbf{u}}\}^n$ by (31).
Step 2. Evaluate acceleration of the free floating subdomains

$$(\tilde{\ddot{\mathbf{u}}})^{n+1} = \hat{\mathbf{M}}^{-1}\left((\mathbf{f})^{n+1} - \mathbf{K}\,(\mathbf{u})_p^{n+1}\right).$$

Step 3. Evaluate acceleration of the frame

$$(\ddot{\mathbf{u}}_{\Gamma})^{n+1} = \mathbf{M}_{\Gamma}^{-1}\,(\mathbf{f}_{\Gamma})^{n+1}.$$

Step 4. Evaluate localized multipliers

$$(\lambda)^{n+1} = \left(\mathbf{M}^{\mathrm{B}\mathsf{T}}\,\mathbf{B}^{\mathsf{T}}\mathbf{M}^{-1}\mathbf{B}\,\mathbf{M}^{\mathrm{B}}\right)^{-1} \cdot \left(\mathbf{M}^{\mathrm{B}\mathsf{T}}\mathbf{B}^{\mathsf{T}}(\tilde{\ddot{\mathbf{u}}})^{n+1} - \mathbf{C}_{\lambda u_{\Gamma}}(\ddot{\mathbf{u}}_{\Gamma})^{n+1}\right).$$

Step 5. Evaluate acceleration of the coupled system

$$(\ddot{\mathbf{u}})^{n+1} = (\tilde{\ddot{\mathbf{u}}})^{n+1} - \mathbf{M}^{-1}\,\mathbf{B}\,\mathbf{M}^{\mathrm{B}}\,(\lambda)^{n+1}.$$

Step 6. Correct $\{\mathbf{u}, \dot{\mathbf{u}}\}_p^{n+1}$ to $\{\mathbf{u}, \dot{\mathbf{u}}\}^{n+1}$ by (33).

Alg. 1. Solution of the global system.

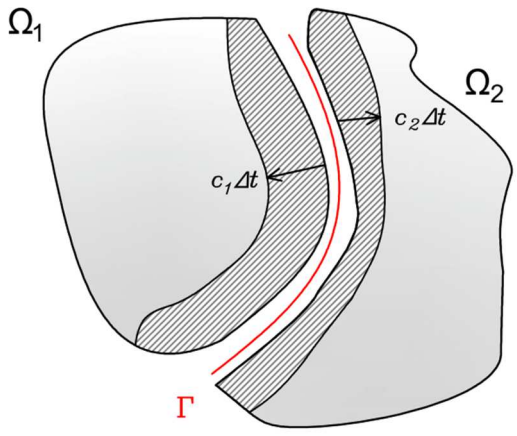

Fig. 3. Domain of dependence/influence of the frame.

$$\begin{bmatrix} \overline{\mathbf{K}}^{\mathbf{r}} & \mathbf{B}^{\mathbf{r}}\,\mathbf{M}^{\mathbf{B}} & \mathbf{0} \\ \mathbf{M}^{\mathbf{B}^{\mathrm{T}}}\mathbf{B}^{\mathbf{r}\,\mathbf{T}} & \mathbf{0} & -\mathbf{C}_{\boldsymbol{\lambda} u_{\Gamma}} \\ \mathbf{0} & -\mathbf{C}^{\mathbf{T}}_{\boldsymbol{\lambda} u_{\Gamma}} & \mathbf{0} \end{bmatrix} \begin{Bmatrix} \mathbf{u}^{\mathbf{r}} \\ \boldsymbol{\lambda} \\ \mathbf{u}_{\Gamma} \end{Bmatrix} = \begin{Bmatrix} \mathbf{f}^{\mathbf{r}} \\ \mathbf{0} \\ \mathbf{0} \end{Bmatrix}, \tag{37}$$

where,

$$\overline{\mathbf{K}}^{\mathbf{r}} = \mathbf{M}^{\mathbf{r}}\,\mathrm{D}^2 + \mathbf{K}^{\mathbf{r}}\,, \qquad \mathrm{D} = \frac{\mathrm{d}}{\mathrm{d}t}\,,$$

where,

$$\mathbf{K}^{\mathbf{r}} = \mathbf{R}\,\mathbf{K}\,\mathbf{R}^{\mathrm{T}}\,, \qquad \mathbf{M}^{\mathbf{r}} = \mathbf{R}\,\mathbf{M}\,\mathbf{R}^{\mathrm{T}}\,, \qquad \mathbf{f}^{\mathbf{r}} = \mathbf{R}\,\mathbf{f}\,, \qquad \mathbf{B}^{\mathbf{r}} = \mathbf{R}\,\mathbf{B} \tag{38}$$

are interface region stiffness and mass matrix, interface region load vector, and interface region boolean operator, respectively. This reduced problem contains frame and adjacent interface regions (see Fig. 4).

Since Eq. (37) is formally the same system as the original one in Eq. (9), we would follow the same approach in its solution.

7. Problem of Drifting

Drifting is a phenomenon in which displacement continuity between subdomains is gradually lost due to the use of time derivatives of the constraint equations. Since contemporary integrators for decomposed models employ either the first or the second derivative of the displacement constraints, drifting is a common feature of such methods. However, in 2019, Cho et al. [20] introduced a technique for avoiding drifting at the cost of a slight violation of the equations of motion. Cho's (and ours) kinematic constraints have the form:

$$\mathbf{M}^{\mathrm{B}^{\mathrm{T}}}\mathbf{B}^{\mathrm{T}}\,\ddot{\mathbf{u}} - \mathbf{C}_{\lambda u_{\Gamma}}\,\ddot{\mathbf{u}}_{\Gamma} = \mathbf{0}\,, \tag{39}$$

so at each end of the computational time step Δt the acceleration continuity is satisfied automatically. However, displacement and velocity suffer from drifting, so Cho suggested the a posteriori correction of the fields:

$$\begin{aligned} \mathbf{u} &= (\mathbf{I} - \mathbf{B}\,\mathbf{B}^{\mathrm{T}})\,\mathbf{u} + \left(\mathbf{B}\,\mathbf{M}^{\mathrm{B}^{\mathrm{T}^{-1}}}\mathbf{C}_{\lambda u_{\Gamma}}\right)\mathbf{u}_{\Gamma}\,, \\ \dot{\mathbf{u}} &= (\mathbf{I} - \mathbf{B}\,\mathbf{B}^{\mathrm{T}})\,\dot{\mathbf{u}} + \left(\mathbf{B}\,\mathbf{M}^{\mathrm{B}^{\mathrm{T}^{-1}}}\mathbf{C}_{\lambda u_{\Gamma}}\right)\dot{\mathbf{u}}_{\Gamma}\,, \end{aligned} \tag{40}$$

which leads to the exact fulfillment of the interface kinematic constraints:

$$\begin{aligned} \mathbf{M}^{\mathrm{B}^{\mathrm{T}}}\mathbf{B}^{\mathrm{T}}\,\mathbf{u} - \mathbf{C}_{\lambda u_{\Gamma}}\,\mathbf{u}_{\Gamma} &= \mathbf{0}\,, \\ \mathbf{M}^{\mathrm{B}^{\mathrm{T}}}\mathbf{B}^{\mathrm{T}}\,\dot{\mathbf{u}} - \mathbf{C}_{\lambda u_{\Gamma}}\,\dot{\mathbf{u}}_{\Gamma} &= \mathbf{0} \end{aligned} \tag{41}$$

at the end of each computational time step Δt, for the slight violation of the equation of motion:

$$\mathbf{M}\,\ddot{\mathbf{u}} + \mathbf{K}\,\mathbf{u} = \mathbf{f} - \mathbf{B}\,\mathbf{M}^{\mathrm{B}}\,\boldsymbol{\lambda}\,. \tag{42}$$

Such a technique may bring certain instability into the solution and has not been adequately investigated, although we have shown, it is working for particular cases [23]. Other approaches may treat the problem with full control of the stability.

Within this work we do not solve the problem of drifting, hence we let the displacement field discontinuity appear within the interface, while monitoring it.

8. Asynchronous Scheme

The asynchronous time scheme is implemented as follows:

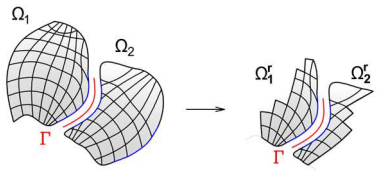

Fig. 4. The transformation of subdomains problem to multiple isolated interface regions problem.

1. INITIALIZATION

1.1. Set the subdomain time vector

$$\mathbf{t} = \{t_1, t_2\} = \mathbf{0}$$

and frame time

$$t_{\Gamma} = 0\,.$$

1.2. Initialize the interface regions

for $i = 1, 2$

$\{\mathbf{u}^{\mathbf{r}}, \dot{\mathbf{u}}^{\mathbf{r}}, \ddot{\mathbf{u}}^{\mathbf{r}}\}_i = \mathbf{R}_i\{\mathbf{u}, \dot{\mathbf{u}}, \ddot{\mathbf{u}}\}_i$

end

1.3. Identify the nearest desired subdomain time levels to solve $\mathbf{t}^{n+1} = \mathbf{t} + \Delta\mathbf{t}$, where $\Delta\mathbf{t} = \{\Delta t_1, \Delta t_2\}$ is vector of computational time steps.

Alg. 2. Initialization of the asynchronous scheme.

From now, at any state of the time integration, there is always the possibility to solve the Frame or at least one of the Subdomains:

- Frame $\mathbf{\Gamma}$ is solvable, when:

$$(t_1^{n+1} > t_\Gamma) \wedge (t_2^{n+1} > t_\Gamma) \ ,$$

i.e., both subdomains have nearest not-yet-known solution after latest already-known solution of the frame. Then the frame is solvable and can be integrated with the frame time step given as:

$$\Delta t_\Gamma = \min\{(t_1^{n+1} - t_\Gamma), (t_2^{n+1} - t_\Gamma)\} \ .$$

- Subdomain is solvable, when:

$$t_i^{n+1} = t_\Gamma \ ,$$

i.e., frame has already known solution at the subdomain's time of interest. Then the subdomain $\mathbf{\Omega}_i$ is solvable and can be integrated with its computational timestep Δt_i.

2.A SOLUTION OF SOLVABLE FRAME

2.A.1. If the frame is solvable, proceed with following subroutine. Otherwise proceed with subroutine **2.B**.

2.A.2. Determine frame timestep

$$\Delta t_\Gamma = \min\{\mathbf{t}^{n+1} - t_\Gamma\}$$

2.A.3. (a) for $\Omega_1^{\mathbf{r}}, \Omega_2^{\mathbf{r}}$ at time $t_\Gamma + \Delta t_\Gamma$ {

i. Predict $\{\mathbf{u}^{\mathbf{r}}, \dot{\mathbf{u}}^{\mathbf{r}}\}_p$

ii. Evaluate $\tilde{\ddot{\mathbf{u}}}^{\mathbf{r}} = \hat{\mathbf{M}}^{\mathbf{r}\,-1}(\mathbf{f}^{\mathbf{r}} - \mathbf{K}^{\mathbf{r}}\,\mathbf{u}_p^{\mathbf{r}})$

}

(b) Evaluate $\ddot{\mathbf{u}}_\Gamma = \mathbf{M}_\Gamma^{-1}\,\mathbf{f}_\Gamma$

(c) for $\Omega_1^{\mathbf{r}}, \Omega_2^{\mathbf{r}}$ {

i. Evaluate

$$\lambda_i = \left(\mathbf{B}_i^{\mathsf{T}}\mathbf{M}_i^{-1}\mathbf{B}_i\right)^{-1} \cdot \left(\mathbf{B}_i^{\mathbf{r}\mathsf{T}}\tilde{\ddot{\mathbf{u}}}_i^{\mathbf{r}} - \mathbf{C}_{\lambda_i u_\Gamma}\ddot{\mathbf{u}}_\Gamma\right) .$$

ii. Evaluate

$$\ddot{\mathbf{u}}_i^{\mathbf{r}} = \tilde{\ddot{\mathbf{u}}}_i^{\mathbf{r}} - \mathbf{M}_i^{\mathbf{r}\,-1}\,\mathbf{B}_i^{\mathbf{r}}\,\lambda_i \, .$$

iii. Correct $\{\mathbf{u}^{\mathbf{r}}, \dot{\mathbf{u}}^{\mathbf{r}}\}_p$ to $\{\mathbf{u}^{\mathbf{r}}, \dot{\mathbf{u}}^{\mathbf{r}}\}$

}

(d) $t_\Gamma = t_\Gamma + \Delta t_\Gamma$

}

Alg. 3. Frame solution.

2.B SOLUTION OF SOLVABLE SUBDOMAINS

2.B.1 If a subdomain Ω_i is solvable, proceed with following subroutine.

2.B.2 for Ω_i at time $t_i + \Delta t_i$ {

(a) Predict $\{\mathbf{u}_i, \dot{\mathbf{u}}_i\}_p$

(b) Evaluate $\tilde{\ddot{\mathbf{u}}}_i = \hat{\mathbf{M}}_i^{-1}(\mathbf{f}_i - \mathbf{K}_i\,(\mathbf{u}_i)_p)$

(c) Evaluate

$$\ddot{\mathbf{u}}_i = \tilde{\ddot{\mathbf{u}}}_i - \mathbf{M}_i^{-1}\,\mathbf{B}_i\,\mathbf{C}_{u\lambda_i}\,\lambda_i$$

(d) Correct $\{\mathbf{u}_i, \dot{\mathbf{u}}_i\}_p$ to $\{\mathbf{u}_i, \dot{\mathbf{u}}_i\}$

(e) Reset interface region $\Omega_i^{\mathbf{r}}$

$$\{\mathbf{u}_i^{\mathbf{r}}, \dot{\mathbf{u}}_i^{\mathbf{r}}, \ddot{\mathbf{u}}_i^{\mathbf{r}}\} = \mathbf{R}_i\{\mathbf{u}_i, \dot{\mathbf{u}}_i, \ddot{\mathbf{u}}_i\} \, .$$

(f) $t_i = t_i + \Delta t_i$ and $t_i^{n+1} = t_i^{n+1} + \Delta t_i$

}

Alg. 4. Subdomain solution.

3. TERMINATION CONDITION

if $\min\{\mathbf{t}\} < T$, repeat phases **2.A** and **2.B**, *else* terminate.

Alg. 5. Termination of the asynchronous scheme.

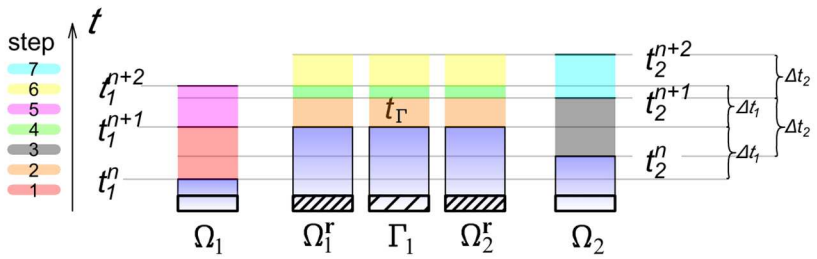

Fig. 5. Steps of asynchronous integration of given problem starting at t_1^n, t_2^n, t_Γ.

If we denote the stated sequence as one step of asynchronous integration, we can illustrate the process of the computation as represented in Fig. 5.

9. Computational Analysis

We set up theoretical test which represents problem of coupling of two problems of different scales (see Fig. 6). The subdomain 1 is represented by small scale cube undergoing explicit DTI (i.e. projectile) and subdomain 2 is big scale cube with considerably more degrees of freedom (impacted body). The subdomains share boundaries with non-matching mesh (see Fig. 7(a)). The interface regions, which are essential for asynchronous integration, are shown (see Fig. 7(b)) for the particular values of safety factors ϵ_i.

Homogeneous material is used:

$$E_1 = E_2 = 1 \text{ Pa} \,, \qquad \nu_1 = \nu_2 = 0 \,, \qquad \rho_1 = \rho_2 = 1 \text{ kg} \cdot \text{m}^{-3} \,. \tag{43}$$

Homogeneous initial conditions $\mathbf{u_0} = \mathbf{v_0} = \mathbf{0}$ are prescribed.

Top face of subdomain 1 is loaded by piece-wise linear pressure pulse:

$$p(t) = \begin{cases} \dfrac{t}{100} & t \leq 100 \text{ s} \,, \\ \dfrac{200 - t}{100} & 100 \text{ s} < t \leq 100 \text{ s} \,, \\ 0 & 200 \text{ s} < t \,. \end{cases}$$

Four outputs are measured within each example:

- point velocities v_z of both subdomain 1 and 2 centers of the mass,
- total energy and,
- drift $\|\Delta u\|$, which is measured as the norm of the first equation in Eq. (41).

The critical time steps are given by the highest eigen frequencies as:

$$\Delta t_1^c = 0.54 \text{ s} \,, \qquad \Delta t_2^c = 4.73 \text{ s} \,. \tag{44}$$

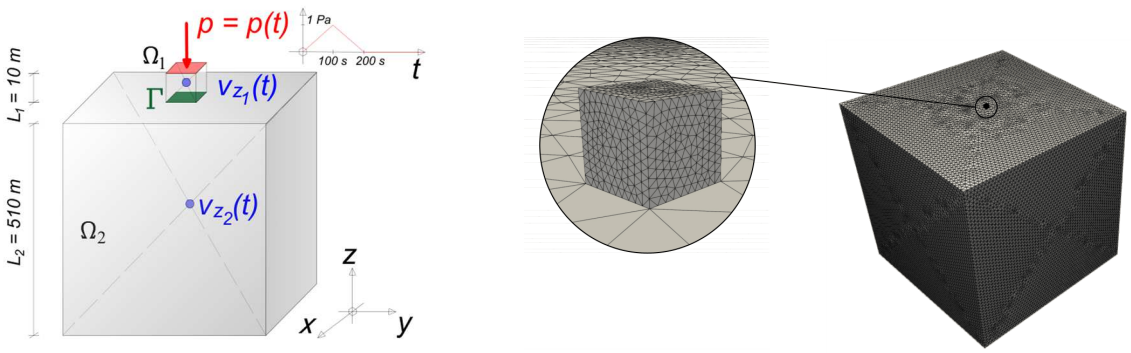

Fig. 6. General problem of connecting two different scales geometry-scheme on the left, real meshed model on the right-small subdomain 1 with fine mesh (5 736 DoFs) and few degrees of freedom attached to the center of top side of the subdomain 2 with rough mesh (620 250 DoFs) but many degrees of freedom.

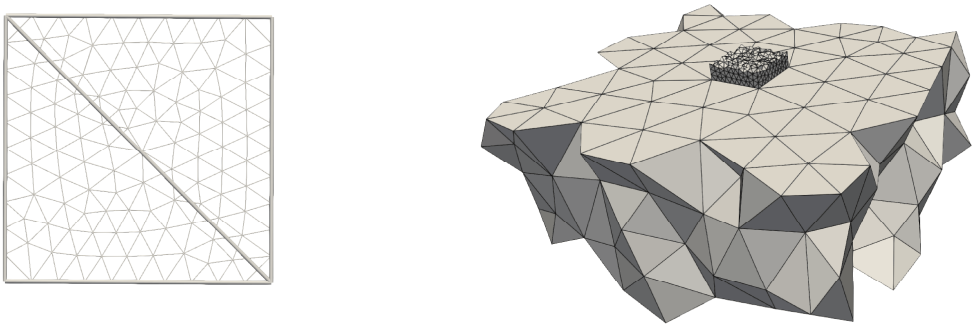

(a) Shared boundaries - thin lines subdomain 1, thick lines subdomain 2.

(b) Isolated frame problem - interface regions for $\epsilon_1 \approx \epsilon_2 \approx 3$.

Fig. 7. Detail of the coupling.

Within the following Examples we use terms *explicit* and *implicit* computation:

- by *explicit* is meant
  - central difference scheme and
  - lumped mass matrix,
- by *implicit* is meant
  - average acceleration scheme and
  - consistent mass matrix.

The frame problem with attached interface regions is always computed *explicitly*. Subdomains undergo *explicit-explicit*, *implicit-implicit* and *explicit-implicit* analysis.

9.1. Example 1: explicit-explicit solution with considerable solution speed up

This example investigates the behavior of the proposed asynchronous framework in the case where both subdomains are integrated using the explicit central difference method. The objective is to verify the accuracy, energy conservation properties, and computational efficiency of the asynchronous formulation when different local time steps are employed. A schematic representation of the analyzed problem is shown in Fig. 8.

9.1.1. *Comparison of the velocities measured at the centers of the cubes*

Using the asynchronous scheme with unified time steps $\Delta t_1 = \Delta t_2 = 0.9 \, . \, \Delta t_1^c$ leads to results that are nearly identical to the LS-DYNA solution (see Fig. 9). The asynchronous solution with individual time steps $\Delta t_1 = 0.9 \, . \, \Delta t_1^c$ and $\Delta t_2 = 0.9 \, . \, \Delta t_2^c$ produces an identical solution in the first subdomain (see Fig. 9(a)), while a slight time shift can be observed in the second subdomain (see Fig. 9(b)). This behavior is typical for FEM simulations when the computational time step is increased.

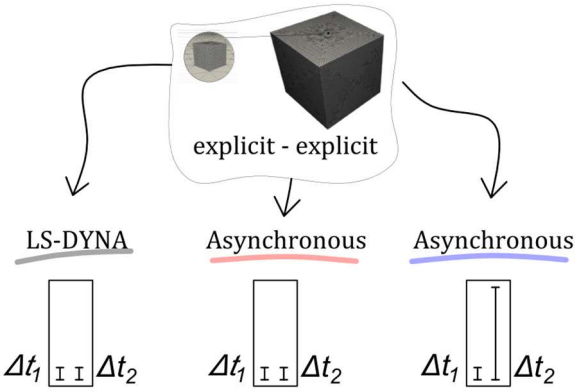

Fig. 8. Setup of example 1.

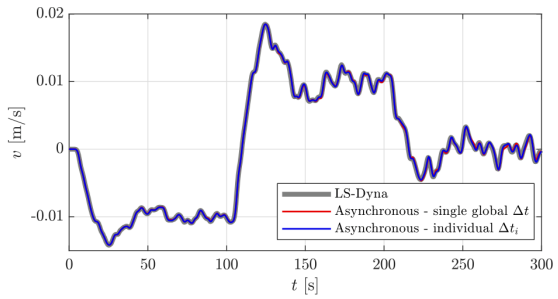

(a) Subdomain 1

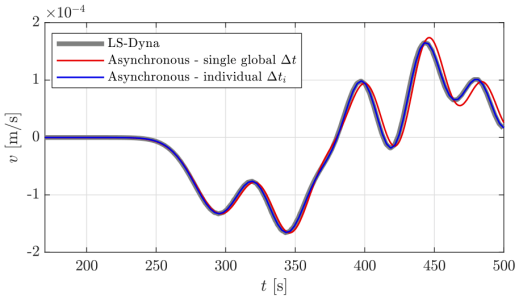

(b) Subdomain 2

Fig. 9. Velocity probes the center of mass of the cubes.

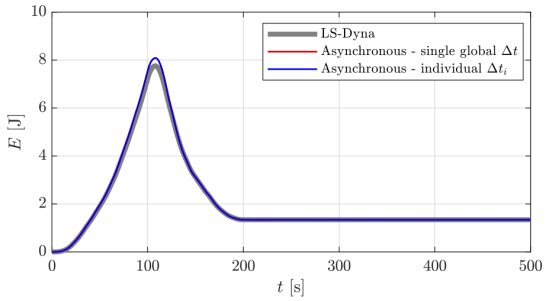

(a) Total energy

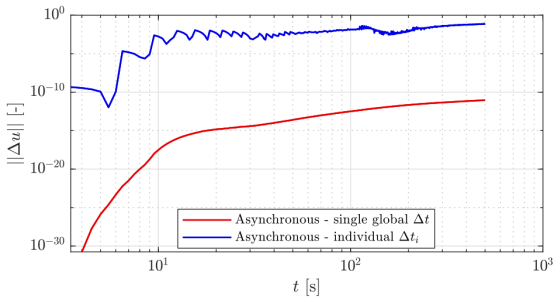

(b) Norm of the displacement drift

Fig. 10. Evolution of global variables.

9.1.2. *Energy balance and drift*

No energy loss is observed in either computation (see Fig. 10(a)). As expected, displacement drift is present (see Fig. 10(b)).

9.1.3. *Algorithm performance*

The principal advantage of the asynchronous solution is its computational efficiency (see Fig. 17(a)) – 436 s (LS-DYNA) versus 109 s for the asynchronous solution with individual time steps.

9.2. Example 2: Explicit-implicit accuracy distortion by drifting

This example investigates the behavior of the proposed asynchronous framework when the first subdomain is integrated explicitly, while the second subdomain is treated using an implicit integration scheme. The objective is to analyze the influence of mixed explicit-implicit coupling on the solution accuracy and on the drifting between subdomains. A schematic representation of the analyzed problem is shown in Fig. 11.

9.2.1. *Comparison of the velocities measured at the centers of the cubes*

The explicit-implicit results for the first subdomain are compared with the explicit-explicit solution (see Fig. 12(a)), while the explicit-implicit results for the second subdomain are compared with the implicit-implicit solution (see Fig. 12(b)). The time steps are fixed across all methods as $\Delta t_1 = 0.9 \cdot \Delta t_1^c$ and $\Delta t_2 = 0.9 \cdot \Delta t_2^c$.

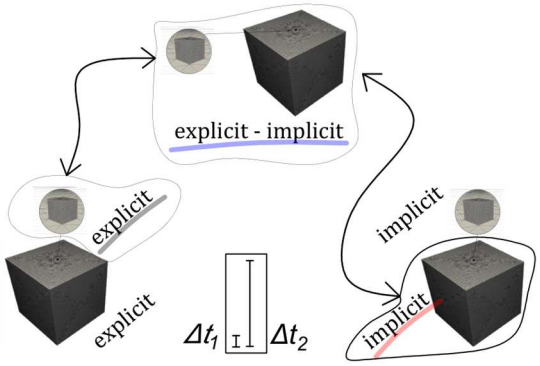

Fig. 11. Setup of example 2.

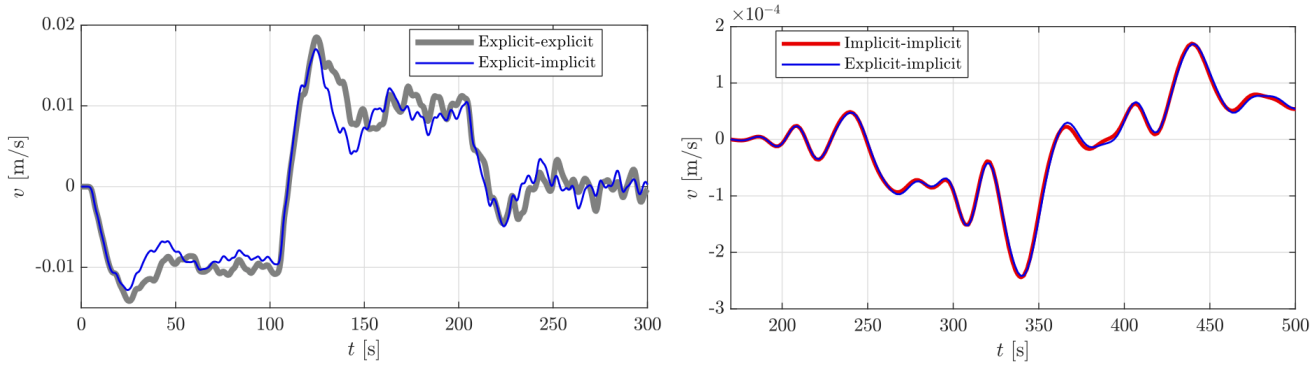

(a) Subdomain 1 (b) Subdomain 2

Fig. 12. Velocity probes the center of mass of the cubes.

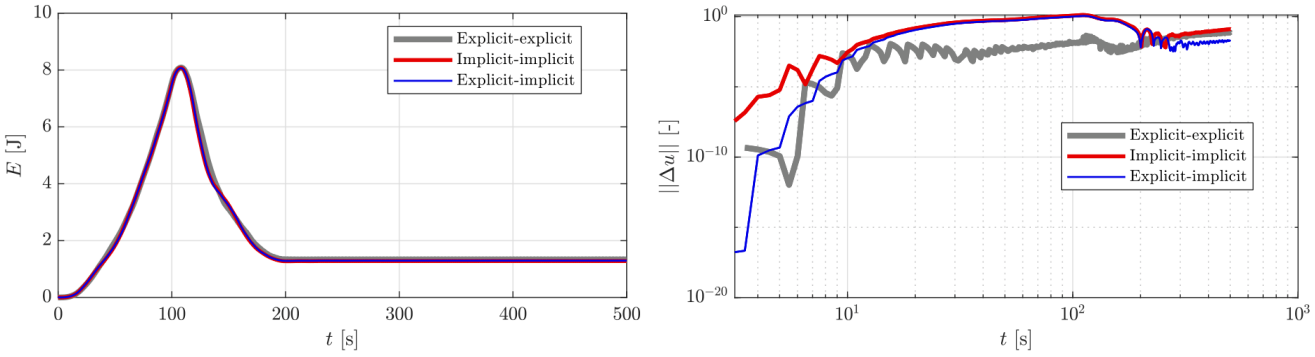

(a) Total energy (b) Norm of the displacement drift

Fig. 13. Evolution of global variables.

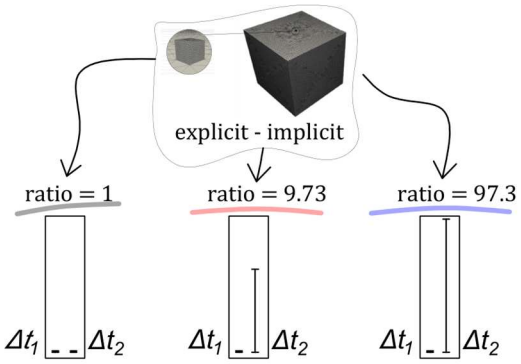

Fig. 14. Setup of example 3.

9.2.2. *Energy balance and drift*

No energy loss is observed in any of the computations (see Fig. 13(a)). However, the displacement drift is significant and exhibits very similar behavior in both the implicit-implicit and explicit-implicit cases when compared to the explicit-explicit solution (see Fig. 13(b)). It is very likely that this drifting distorts the explicit solution of the first subdomain (see Fig. 12(a)).

9.3. Example 3

This example focuses on the computational efficiency of the proposed explicit-implicit asynchronous framework for increasing ratios between the local time steps. Although the previous examples demonstrated the presence of drifting during explicit-implicit coupling, several techniques have been proposed to mitigate this issue (see Sec. 7), with successful application in particular cases. Therefore, the primary objective of the present example is to highlight the computational speedup enabled by the proposed asynchronous strategy.

9.3.1. *Comparison of the velocities measured at the centers of the cubes*

A set of three explicit-implicit analyses is performed with progressively increasing time-step ratios. The first subdomain is always integrated explicitly using as $\Delta t_1 = 0.9 \cdot \Delta t_1^c$, while the second subdomain is integrated implicitly with increasing time steps as $\Delta t_2 = \{\Delta t_1, \Delta t_2^c, 10\Delta t_2^c\}$. The effect of the large time step can be clearly observed in the blue curve - the large subdomain is no longer able to capture all physical details accurately, while simultaneously distorting the solution in the first subdomain.

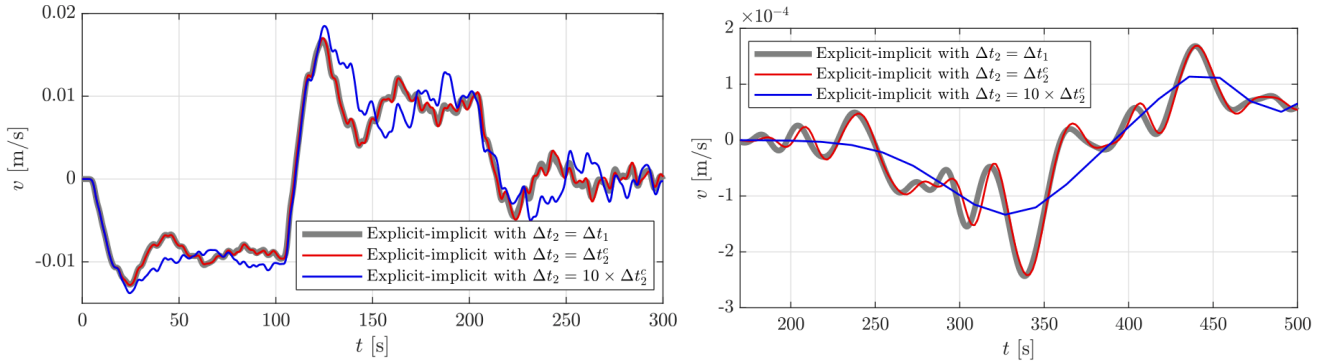

(a) Subdomain 1 (b) Subdomain 2

Fig. 15. Velocity probes the center of mass of the cubes.

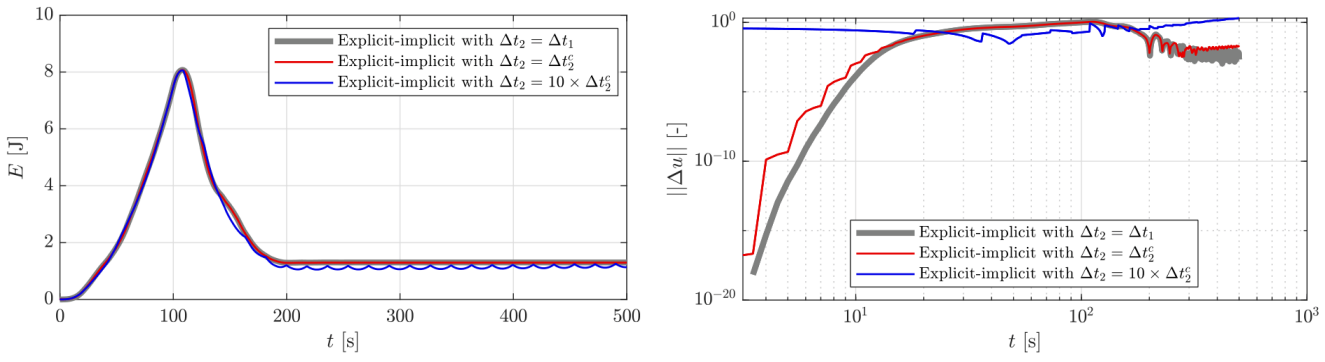

(a) Total energy (b) Norm of the displacement drift

Fig. 16. Evolution of global variables.

9.3.2. *Energy balance and drift*

No apparent energy loss is observed in any of the computations (see Fig. 16(a)). The distortion visible in the blue solution is caused by the interpolation of sparse results from the second subdomain. The drift effect increases with increasing time step (see Fig. 16(b)).

9.3.3. *Algorithm performance*

The corresponding solution times are 3147 s, 724 s, and 160 s, respectively (see Fig. 17(b)), demonstrating the substantial computational savings achieved by the asynchronous approach.

10. Conclusion

This paper is extended study of previously proposed integrator [23]. Within this paper, we demonstrate the usage for explicit-implicit analysis and give some details on time of solution. The key idea of our scheme is treating the interface as an isolated problem with adjacent interface regions. The interface problem is always solved explicitly.

Presented asynchronous scheme has the potential to be a robust and accurate once the problem of displacement drifting is solved. Then it may be used for mixed problems of explicit and implicit dynamics in any combination. At this point, the scheme is reliable for explicit-explicit problems, where we have proven that results match solution of commercial software (LS-Dyna), however, in shorter solution time (see Fig. 17(a)). Even though we find this remarkable, the speed up of the solution is enormous in explicit-implicit case (see Fig. 17(b)).

Let us itemize these two main outcomes and give a little more detail and explanation:

- In case of explicit-explicit formulation, since the mass matrices of both subdomains are diagonal, solution of the system at each time step is highly efficient and not enormously more time expensive than other procedures during time integration, although still the most expensive one in the process. Therefore, we obtain moderate speed up of the solution when solved asynchronously, while having the problem of one subdomain with few degrees of freedom and short time step the other with many degrees of freedom and long timestep (that is exactly out theoretical example). On the other hand, assuming we have two subdomains with comparable degrees of freedom, the asynchronous time integration may not bring major speed up of the solution.
- In case of explicit-implicit formulation, the speed up is enormous, because the second subdomain has many degrees of freedom when compared to the first one and has consistent mass matrix. Therefore, solution of this system is very time expensive compared to the other procedures during time integration. Classical global step time integration enforces the solution of equation of motion at every time level of subdomain 1. Asynchronous approach allows us to reduce number of these solutions while preserving accuracy. For the cost of losing accuracy, we can even increase the time step ration in order to speed up the solution.

As a major drawback, drifting is observed, which is, however, also common in other existing coupling methods. In particular, implicit time integration schemes introduce numerical damping, which may alter the dynamic response and lead to a gradual mismatch between subdomain solutions and the explicitly integrated interface response, especially in mixed explicit–implicit settings. This effect can potentially contribute to the observed drift, although it is not the sole source of the phenomenon.

Most existing approaches are based on velocity-level coupling, where only displacement drift typically appears. Since the present formulation enforces constraints at the acceleration level, drift can be observed in both displacement and velocity fields. However, during the past, some solutions were offered [20], and we tend to work on this problem in the future.

An interesting and natural extension of the present asynchronous framework is the incorporation of model order reduction techniques within selected subdomains. In addition to coupling different time integration schemes (explicit-implicit), the proposed formulation could in principle be extended to a heterogeneous setting where some subdomains are treated by full finite element discretizations, while others are described in a reduced modal space (e.g., based on modal superposition or component mode synthesis). Such approaches are well established in linear structural dynamics and multi-body systems due to their significant computational efficiency, and their integration into a unified asynchronous coupling strategy represents a promising direction for future research.

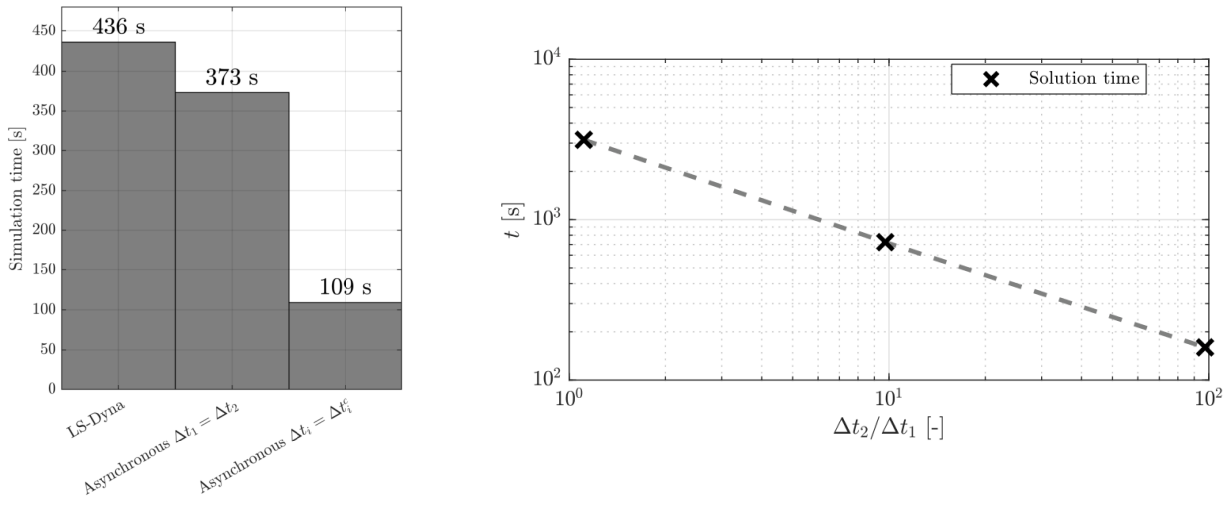

(a) Example 1 (b) Example 3

Fig. 17. Speed up of the solution in explicit-explicit analysis when integrated asynchronously (left) and explicit-implicit problem with increasing time step ratio (right).

Author Contributions

Both authors contributed equally.

Acknowledgments

The first author was supported by project No. 25-18209S of the Czech Science Foundation and by institutional support RVO:61388998 within Institute of Thermomechanics of the CAS.

Computational resources were provided by the e-INFRA CZ project (ID:90254), supported by the Ministry of Education, Youth and Sports of the Czech Republic.

Conflict of Interest

The authors declared no potential conflicts of interest concerning the research, authorship, and publication of this article.

Funding

The authors received no financial support for the research, authorship, and publication of this article.

Data Availability Statements

The datasets generated and/or analyzed during the current study are available from the corresponding author on reasonable request.

Nomenclature

$\mathbf{B}$	Boolean operator	$\mathbf{n}$	Normal vector
$\mathbf{B^r}$	Interface region Boolean operator	p	Pressure [Pa]
$\boldsymbol{b}$	Intensity of volume forces [N m^{-3}]	$\mathbf{R}$	Reducing operator
$\mathbf{C}_{\lambda u_\Gamma}$	Domain-frame coupling operator	t	Time [s]
$\mathbf{D}$	Material matrix	$\boldsymbol{t}$	Traction vector
E	Young modulus [Pa]	$\mathcal{T}$	Kinetic energy [J]
$\mathbf{f}$	Nodal force vector	$\boldsymbol{u}$	Field of domain displacement
$\mathbf{f^r}$	Interface region force vector	$\mathbf{u}$	Nodal domain displacement vector
$\mathbf{K}$	Stiffness matrix	$\tilde{\ddot{\mathbf{u}}}$	Acceleration predictor
$\mathbf{K^r}$	Interface region Stiffness matrix	$\mathbf{u_0}$	Initial displacement
$\boldsymbol{\ell}$	Field of Lagrange multipliers	$\boldsymbol{u}_\Gamma$	Field of frame displacement
$\mathbf{M}$	Mass matrix	u_Γ	Nodal frame displacement vector
$\mathbf{M^r}$	Interface region mass matrix	$\mathcal{U}$	Potential energy [J]
$\mathbf{M}^{\mathrm{B}}$	Surface mass matrix	v	Velocity [m s^{-1}]
$\mathbf{M}_{12}$	Coupling operator of nonmatching meshes	$\mathbf{v_0}$	Initial velocity
$\mathbf{N}_{u_i}$	Subdomain displacement shape function	$\mathcal{W}$	Work [J]
$\mathbf{N}_{u_\Gamma}$	Frame displacement shape function	$\mathcal{W}_\Gamma$	Work of interface constraints [J]
$\mathbf{N}_{\lambda_i}$	Lagrange multipliers shape function	$\boldsymbol{x}$	Coordinates [m]
β, γ	Newmark parameters	ν	Poisson ratio [-]
ϵ	Safety factor of interface region	$\boldsymbol{\Omega}$	Domain
$\boldsymbol{\varepsilon}$	Strain tensor	$\boldsymbol{\Omega}_i$	i-th subdomain
$\boldsymbol{\Gamma}$	Frame	$\boldsymbol{\Omega}_i^{\mathbf{r}}$	i-th interface region
Δt_i	Computational timestep of subdomain i [s]	ρ	Mass density [kg m^{-3}]
Δt_i^c	Critical timestep of subdomain i [s]	$\boldsymbol{\sigma}$	Stress tensor
$\boldsymbol{\lambda}$	Nodal Lagrange multipliers vector		

References

[1] Marinkovic, D., Zehn, M., Survey of finite element method-based real-time simulations, *Applied Sciences*, 9, 2019, 2775.

[2] Hughes, T.J.R., The Finite Element Method: Linear Static and Dynamic Finite Element Analysis, Dover Publications, 2000.

[3] Wen, W.B., He, L., Liu, T., Deng, S., Duan, S., A novel hybrid sub-step explicit time integration method with cubic B-spline interpolation and momentum corrector technique for linear and nonlinear dynamics, *Nonlinear Dynamics*, 110, 2022, 2685-2714.

[4] Wen, W.B., Hong, Y., Wang, P., A generalized three-sub-step composite implicit time integration method with improved accuracy and convergence for linear and nonlinear dynamics, *International Journal of Structural Stability and Dynamics*, 2025.

[5] Gander, M.J., Vandewalle, S., Analysis of the parareal time-parallel time-integration method, *SIAM Journal on Scientific Computing*, 29, 2007, 556-578.

[6] Falgout, R.D., Manteuffel, T.A., O'Neill, B., Schroder, J.B., Multigrid reduction in time for nonlinear parabolic problems: A case study, *SIAM Journal on Scientific Computing*, 39, 2017, S298-S322.

[7] Belytschko, T., Mullen, R., Mesh partitions of explicit-implicit time integration, Formulations and Computational Algorithms in Finite Element Analysis: U.S.-Germany Symposium, Cambridge, USA, 1977.

[8] Belytschko, T., Mullen, R., Stability of explicit-implicit mesh partitions in time integration, *International Journal for Numerical Methods in Engineering*, 12, 1978, 1575-1586.

[9] Smolinski, P., Subcycling integration with non-integer time steps for structural dynamics problems, *Computers & Structures*, 59, 1996, 273-281.

[10] Daniel, W.J.T., A study of the stability of subcycling algorithms in structural dynamics, *Computer Methods in Applied Mechanics and Engineering*, 156, 1998, 1-13.

[11] Smolinski, P., Sleith, S., Belytschko, T., Stability of an explicit multi-time step integration algorithm for linear structural dynamics equations, *Computational Mechanics*, 18, 1996, 236-244.
[12] Combescure, A., Gravouil, A., A numerical scheme to couple subdomains with different time-steps for predominantly linear transient analysis, *Computer Methods in Applied Mechanics and Engineering*, 191, 2002, 1129-1157.
[13] Faucher, V., Bung, H., Combescure, A., Europlexus: a domain decomposition method in explicit dynamics, International Conference on Supercomputing in Nuclear Applications SNA, Paris, France, 2003.
[14] Prakash, A., Hjelmstad, K.D., A FETI-based multi-time-step coupling method for newmark schemes in structural dynamics, *International Journal for Numerical Methods in Engineering*, 61, 2004, 2183-2204.
[15] Fekak, F.E., Brun, M., Gravouil, A., Depale, B., A new heterogeneous asynchronous explicit–implicit time integrator for nonsmooth dynamics, *Computational Mechanics*, 60, 2017, 1-21.
[16] Chantrait, T., Rannou, J., Gravouil, A., Low intrusive coupling of implicit and explicit time integration schemes for structural dynamics: Application to low energy impacts on composite structures, *Finite Elements in Analysis and Design*, 86, 2014, 23-33.
[17] Gravouil, A., Combescure, A., Brun, M., Heterogeneous asynchronous time integrators for computational structural dynamics, *International Journal for Numerical Methods in Engineering*, 102, 2015, 202-232.
[18] Subber, W., Matouš, K., Asynchronous space–time algorithm based on a domain decomposition method for structural dynamics problems on non-matching meshes, *Computational Mechanics*, 57, 2016, 211-235.
[19] Seibold, A.S., Rixen, D.J., Asynchronous time integration in structural mechanics, *Proceedings in Applied Mathematics and Mechanics*, 19, 2019, e201900495.
[20] Cho, S.S., Kolman, R., González, J.A., Park, K.C., Explicit multistep time integration for discontinuous elastic stress wave propagation in heterogeneous solids, *International Journal for Numerical Methods in Engineering*, 118, 2019, 276-302.
[21] Jadhav, D.B., Phansalkar, D., Weinberg, K., Ortiz, M., Leyendecker, S., A spatio-temporally adaptive asynchronous variational integrator for a phase field model of dynamic fracture, *Mechanics of Materials*, 215, 2026, 105604.
[22] Zhang, K.M., Wexler, A.S., An asynchronous time-stepping (ATS) integrator for atmospheric applications: Aerosol dynamics, *Atmospheric Environment*, 40, 2006, 4574-4588.
[23] Dvořák, R., Kolman, R., Mračko, M., Kopačka, J., Fíla, T., Jiroušek, O., Falta, J., Neuhäuserová, M., Rada, V., Adámek, V., González, J.A., Energy-conserving interface dynamics with asynchronous direct time integration employing arbitrary time steps, *Computer Methods in Applied Mechanics and Engineering*, 413, 2023, 116110.
[24] Park, K.C., Felippa, C.A., A variational framework for solution method developments in structural mechanics, *Journal of Applied Mechanics*, 65, 1998, 242-249.
[25] Park, K.C., Felippa, C.A., A variational principle for the formulation of partitioned structural systems, *International Journal for Numerical Methods in Engineering*, 47, 2000, 395-418.
[26] González, J.A., Kopačka, J., Kolman, R., Park, K.C., Partitioned formulation of contact-impact problems with stabilized contact constraints and reciprocal mass matrices, *International Journal for Numerical Methods in Engineering*, 122, 2021, 4609-4636.
[27] Milić, P., Marinković, D., Ćojbašić, Ž., Geometrically nonlinear analysis of piezoelectric active laminated shells by means of isogeometric FE formulation, *Facta Universitatis, Series: Mechanical Engineering*, 23, 2025, 387-405.
[28] Dvořák, R., González, J.A., On the automatic construction of interface coupling operators for non-matching meshes by optimization methods, *Computer Methods in Applied Mechanics and Engineering*, 432, 2024, 117336.
[29] Park, K.C., Felippa, C.A., Gumaste, U.A., A localized version of the method of Lagrange multipliers and its applications, *Computational Mechanics*, 24, 2000, 476-490.
[30] Park, K.C., Felippa, C.A., Rebel, G., A simple algorithm for localized construction of non-matching structural interfaces, *International Journal for Numerical Methods in Engineering*, 53, 2002, 2117-2142.
[31] Song, Y.U., Youn, S.K., Park, K.C., A gap element for treating non-matching discrete interfaces, *Computational Mechanics*, 56, 2015, 551-563.
[32] Song, Y.U., Youn, S.K., Park, K.C., Virtual gap element approach for the treatment of non-matching interface using three-dimensional solid elements, *Computational Mechanics*, 60, 2017, 585-594.
[33] Song, Y.U., Jeong, G.E., Youn, S.K., Park, K.C., Virtual tetrahedral gap element to connect three-dimensional non-coincident interfaces, *Finite Elements in Analysis and Design*, 152, 2018, 18-26.
[34] Jeong, G.E., Song, Y.U., Youn, S.K., Park, K.C., A new approach for nonmatching interface construction by the method of localized Lagrange multipliers, *Computer Methods in Applied Mechanics and Engineering*, 361, 2020, 112728.

ORCID iD

Radim Dvořák https://orcid.org/0000-0002-4056-4842
Radek Kolman https://orcid.org/0000-0002-8167-3535

How to cite this article: Dvorak R., Kolman R. Numerical Analysis of Asynchronous Time Scheme for Explicit Implicit Problems, *J. Appl. Comput. Mech.*, xx(x), 2026, 1–15. https://doi.org/10.22055/jacm.2026.49215.5812